Combination of cGMP analogue and drug delivery system provides functional protection in hereditary retinal degeneration

Eleonora Vighi[a,1], Dragana Trifunović[b,1], Patricia Veiga-Crespo[c,1], Andreas Rentsch[d,2], Dorit Hoffmann[a,2], Ayse Sahaboglu[b,2], Torsten Strasser[b], Manoj Kulkarni[b,e], Evelina Bertolotti[a], Angelique van den Heuvel[f], Tobias Peters[b], Arie Reijerkerk[f], Thomas Euler[b,e], Marius Ueffing[b], Frank Schwede[d], Hans-Gottfried Genieser[d], Pieter Gaillard[f,g], Valeria Marigo[a,3], Per Ekström[c,3], and François Paquet-Durand[b,3]

[a]Dipartimento di Scienze della Vita, Università degli Studi di Modena e Reggio Emilia, 41125 Modena, Italy; [b]Forschungsinstitut für Augenheilkunde, Department für Augenheilkunde, Eberhard Karls Universität Tübingen, 72076 Tübingen, Germany; [c]Ophthalmology, Department of Clinical Sciences Lund, Faculty of Medicine, Lund University, 22184 Lund, Sweden; [d]BIOLOG Life Science Institute Forschungslabor und Biochemica-Vertrieb GmbH, 28199 Bremen, Germany; [e]Centre for Integrative Neuroscience, Eberhard Karls Universität Tübingen, 72076 Tübingen, Germany; [f]to-BBB technologies BV, 2333 CH Leiden, The Netherlands; and [g]2-BBB Medicines BV, 2333 CH Leiden, The Netherlands

Inherited retinal degeneration (RD) is a devastating and currently untreatable neurodegenerative condition that leads to loss of photoreceptor cells and blindness. The vast genetic heterogeneity of RD, the lack of "druggable" targets, and the access-limiting blood–retinal barrier (BRB) present major hurdles toward effective therapy development. Here, we address these challenges (i) by targeting cGMP (cyclic guanosine- 3′,5′-monophosphate) signaling, a disease driver common to different types of RD, and (ii) by combining inhibitory cGMP analogs with a nanosized liposomal drug delivery system designed to facilitate transport across the BRB. Based on a screen of several cGMP analogs we identified an inhibitory cGMP analog that interferes with activation of photoreceptor cell death pathways. Moreover, we found liposomal encapsulation of the analog to achieve efficient drug targeting to the neuroretina. This pharmacological treatment markedly preserved in vivo retinal function and counteracted photoreceptor degeneration in three different in vivo RD models. Taken together, we show that a defined class of compounds for RD treatment in combination with an innovative drug delivery method may enable a single type of treatment to address genetically divergent RD-type diseases.

PKG | CNG channel | calpain | apoptosis | in vivo imaging

Hereditary retinal degeneration (RD) relates to a group of rare blinding diseases in which the photoreceptors of the retina degenerate and die. RD-type diseases, such as retinitis pigmentosa or Leber's congenital amaurosis, are genetically very heterogeneous and, unfortunately, still untreatable (1, 2). Typically, these diseases first affect rod photoreceptors, which mediate vision under dim-light conditions. Since human vision mostly depends on cone photoreceptors—responsible for high-resolution color vision in bright light—rod-mediated vision is less critical for humans, and indeed many RD patients notice the primary loss of rods only at an advanced disease stage. However, the loss of rods triggers the subsequent loss of cones, which then leads to complete blindness (3). Conversely, the preservation of rods should thus save cone-mediated vision (4).

cGMP (cyclic guanosine- 3′,5′-monophosphate) is a key molecule for photoreceptor signal transduction and has two general cellular effectors: cyclic nucleotide gated ion channels (CNGCs) and cGMP-dependent protein kinase (PKG) (5). In the transduction cycle, photoreceptor cGMP is degraded by phosphodiesterase-6 (PDE6) and accordingly a loss-of-function mutation in the rod-specific *Pde6b* gene causes an excessive accumulation of cGMP in rods, as seen for instance in the *rd1* mouse model for RD (6, 7). This cGMP accumulation brings on rapid rod cell death and eventually secondary loss of cones (8).

Abnormally high levels of cGMP in photoreceptors are a common feature in several genetically different forms of RD (6,

7, 9–13). Moreover, the cGMP effector PKG is overactivated in mutant photoreceptors and experimental PKG activation alone is sufficient to cause photoreceptor death in WT retina (7). The second major cGMP effector, the CNGCs, play an integral role in phototransduction, as they enable the influx of Na$^+$ and Ca^{2+}, linking the transduction cascade to changes in photoreceptor membrane potential. CNGC beta subunit deletion protects *rd1* photoreceptors (14), suggesting that also CNGCs contribute to the disease progression. Here, the mechanism probably involves increased Ca^{2+} influx and subsequent activation of Ca^{2+}-dependent calpain-type proteases (15), including proteolytic activation of apoptosis-inducing factor (AIF) (16). cGMP-dependent overactivation of PKG and CNGC in photoreceptors

Significance

Development of treatments for hereditary degeneration of the retina (RD) is hampered by the vast genetic heterogeneity of this group of diseases and by the delivery of the drug to an organ protected by the blood–retina barrier. Here, we present an approach for the treatment of different types of RD, combining an innovative drug therapy with a liposomal system that facilitates drug delivery into the retina. Using different animal models of RD we show that this pharmacological treatment preserved both the viability of cells in the retina as well as retinal function. Thus, our study provides an avenue for the development of therapies for hereditary diseases which cause blindness, an unmet medical need.

may, thus, qualify as critical disease drivers, making them promising candidates for a targeted molecular intervention therapy for RD (17).

To address the "targetability" of PKG and CNGC we have produced and tested cGMP analogs that inhibit these proteins. We devised a multilevel approach, in which cGMP analogs were designed, synthesized, and then screened in biological systems of increasing complexity. We first investigated cGMP analog effects in photoreceptor-like cells in vitro, then in organotypic retinal explant cultures and acute retinal slice preparations, and finally in vivo. In the living animal, the photoreceptor cells reside behind the blood–retinal barrier (BRB) (18). To overcome this barrier, a liposomal drug delivery vehicle was used, to facilitate transfer of cGMP analogs into the retina (19).

With this workflow, we identified a liposomal (LP) cGMP analog formulation, LP-CN03, which markedly preserved in vivo retinal function and reduced rod photoreceptor loss in three different RD models. Targeting cGMP signaling in this way not only protected rods affected by different causative mutations but also resulted in functional preservation of cones. In combination with liposomal delivery this approach offers a starting point for

the development and translation of a pharmacological therapy with defined molecular targets.

Results

To investigate the potential of cGMP analogs as a new pharmacological class for the treatment of RD we took advantage of the possibilities to modify these compounds so that they could inhibit PKG and/or CNGC.

Development of cGMP Analogs. R_P-configured phosphorothioate-modified cGMP (R_P-cGMPS; *SI Materials and Methods*) analogs are classified as inhibitors of PKG, regardless of other nucleobase modifications (20, 21). The introduction of the β-phenyl-1,N^2-etheno-modification (PET) onto the R_P-cGMPS backbone additionally inhibits photoreceptor CNGC (22). In contrast, R_P-cGMPS analogs with modifications in position 8 (C-8) alone are CNGC activators (23).

We used two parallel strategies for designing R_P-cGMPS analogs (Fig. 1A). First, we employed C-8 substituents either alone or in combination with the PET motif. Second, we evolved alternatives of the PET moiety, containing substituents that
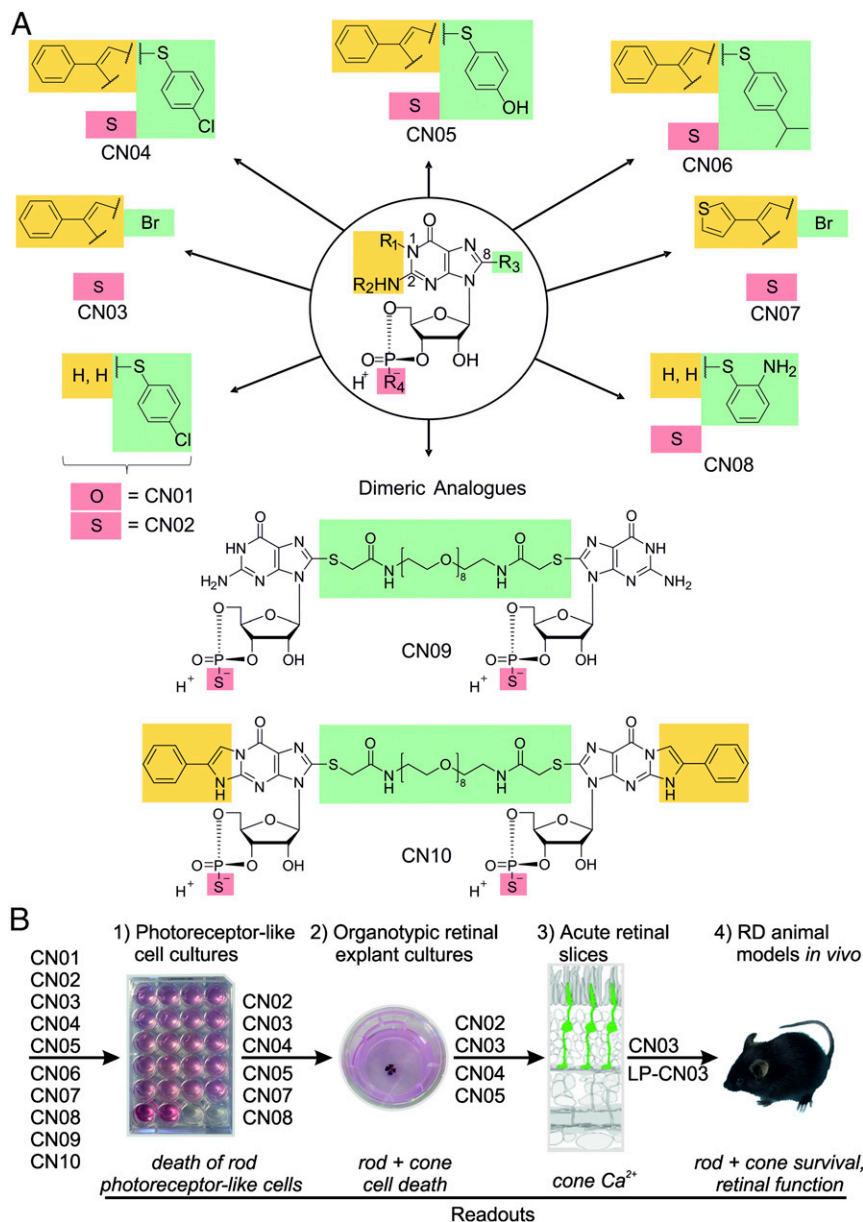
Fig. 1. Structures of mono- and dimeric cGMP analogs and flow chart for biological activity testing. (A) Illustration of monomers is reduced to the modifications introduced. $R_1 + R_2$ (yellow highlight) include the PET modifications, R_3 (green) refers to the 8 position (C-8) of cGMP, and a sulfur atom at R_4 (red) establishes the R_P-configured phosphorothioate. (B) Stepwise compound screening in systems of increasing biological complexity. At each step compounds were filtered out based on photoreceptor-specific readouts, with only CN03 and its liposomal formulation (LP-CN03) reaching the in vivo stage.

Table 1. Lipophilicity data and putative effect of R_P-cGMPS analogs

Compound	Analog	log k'$_g$	rL$_{cGMP}$*	Effect on PKG	Effect on CNGC
A	cGMP	0.770	1.0	+	+
B	R_P-cGMPS	0.894	1.3	−	+
C	R_P-8-Br-cGMPS	1.285	3.3	−	+
CN01	8-pCPT-cGMP	2.520	56	+	+
CN02	R_P-8-pCPT-cGMPS	2.610	69	−	+
CN03	R_P-8-Br-PET-cGMPS	2.831	115	−	−
CN04	R_P-8-pCPT-PET-cGMPS	3.530	575	−	±[†]
CN05	R_P-8-pHPT-PET-cGMPS	3.078	203	−	±[†]
CN06	R_P-8-pIPrPT-PET-cGMPS	3.815	1,109	−	±[†]
CN07	R_P-8-Br-(3-Tp)ET-cGMPS	2.746	95	−	−
CN08	R_P-8-oAPT-cGMPS	1.974	16	−	+
CN09	R_P-cGMPS-8-TMAmd-(EO)$_8$-EAmdMT-8-R_P-cGMPS	2.039[‡]	19	−	+
CN10	PET-R_P-cGMPS-8-TMAmd-(EO)$_8$-EAmdMT-8-R_P-cGMPS-PET	3.236[‡]	292	−	±[†]

"+" indicates a PKG/CNGC activator; "−" indicates inhibitor.
*Relative lipophilicity of R_P-cGMPS analog compared with cGMP.
[†]No distinct assignment as CNGC inhibitor, as large substituents in 8 position tend to activate CNGC and might overrule inhibition induced by PET or PET-like substitution.
[‡]Values for dimeric analogs are not directly comparable with values for monomeric analogs.

connect positions 1 and N^2 of the guanine nucleobase as well as substituents solely bound to position 1. These two strategies led to the generation of a set of R_P-cGMPS structures, most of them with strongly increased lipophilicity compared with the parent compound cGMP (Table 1).

To further improve potency and specificity, a strategy originally described for activatory cGMP-analogs (24) was extended to inhibitory cGMP analogs, where a polymer- (e.g., PEG) linked dimer with equal or different R_P-cGMPS analogs at its ends formed a so-called spanning clamp (Fig. 1A). Such inhibitory clamps are expected to simultaneously block two cGMP binding sites of CNGC or PKG by using a combination of PET- and 8-substituents with correspondingly slow off-rates after binding (24).
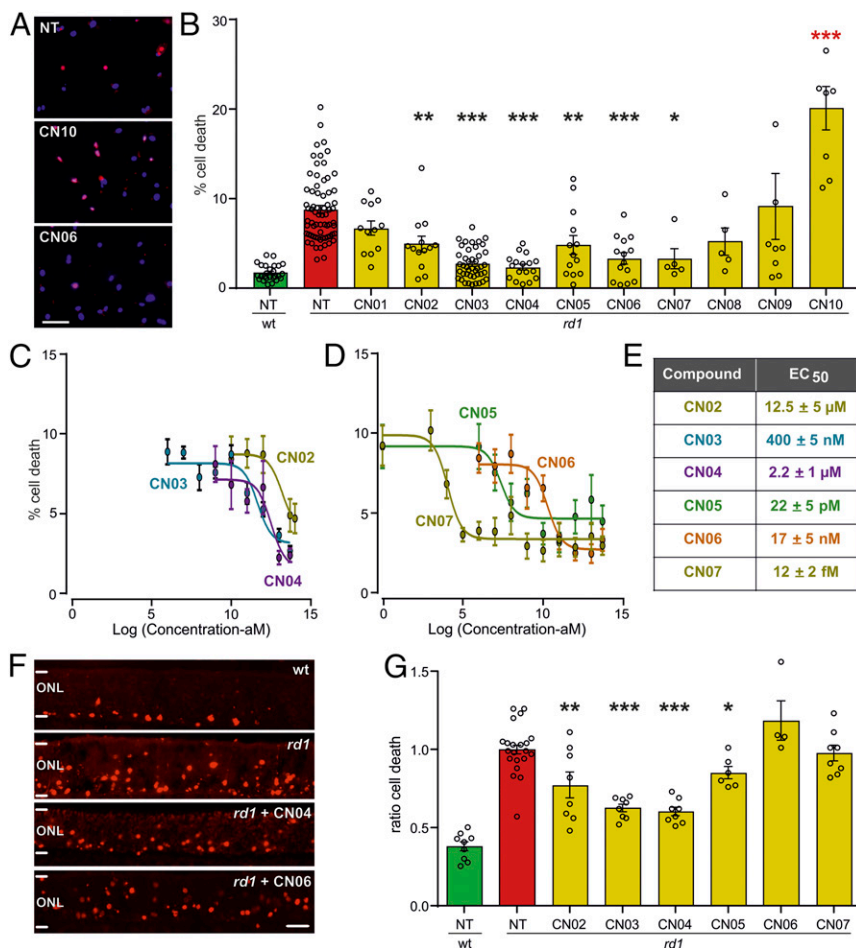

Fig. 2. Screening of cGMP analogs in vitro. cGMP analogs were tested in retinal neurosphere-derived rod photoreceptor-like cell cultures (A–E) and organotypic retinal explant cultures (F and G). NT, not treated. (A) rd1 mutant photoreceptor-like cell cultures treated with 50 μM of the respective compound until DIV11 (red, ethidium homodimer staining; blue, nuclear counter staining). (B) Percentage of ethidium homodimer-labeled, dying photoreceptor-like cells [green, WT; red, rd1; yellow, different analog treatments; n = 5–62 cell culture samples obtained from two to seven independent preparations; red asterisks indicate toxic effect (i.e., more dying cells compared with NT)]. (C and D) Dose–response curves for CN02–CN07 starting at attomolar concentration. (E) EC$_{50}$ values for CN02–CN07 calculated from dose–response curves. (F) TUNEL assay (red) on vertical sections from P11 retinal cultures NT or treated with 50 μM of the respective compound. (G) Ratio (treated/NT) of TUNEL-labeled cells (same color code as in B, WT, n = 9 separate retinal explant cultures; rd1: NT, 22; CN02, 8; CN03, 8; CN04, 8; CN05, 6; CN06, 4; CN07, 8). Error bars: SEM. Statistical comparisons: B and G, NT-rd1 vs. treated rd1 using one-way ANOVA with Holm–Šidak's multiple-comparisons test; ONL, outer nuclear layer containing rod and cone photoreceptor nuclei. (Scale bars: A, 100 μm; F, 50 μm.) *$P \leq 0.05$, **$P \leq 0.01$, ***$P \leq 0.001$.
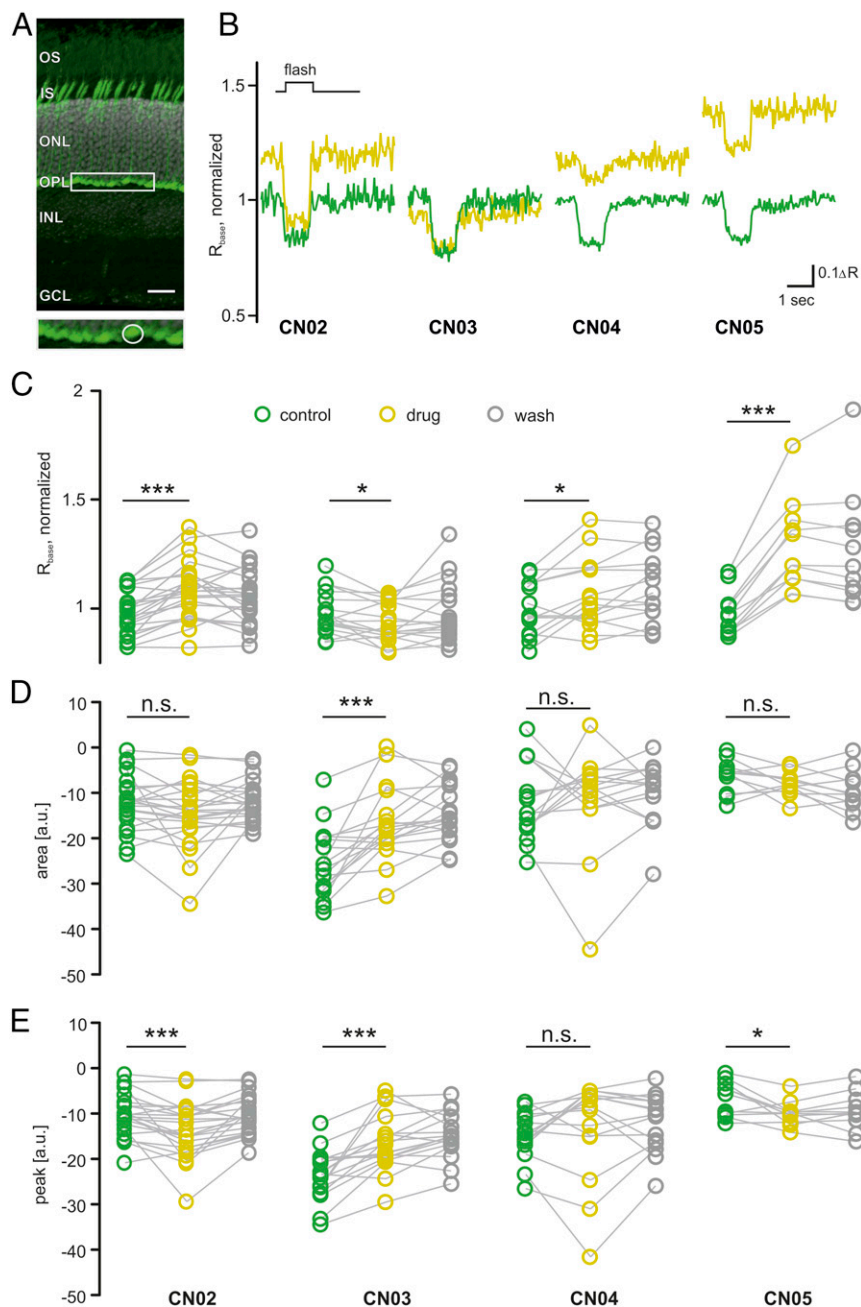
Fig. 3. Effects of cGMP analogs on cone photoreceptor Ca²⁺ dynamics. (*A*) Vertical section of a mouse retina, expressing the TN-XL Ca²⁺ biosensor (below: magnification of cone terminals, indicated by box in top image). (Scale bar: 20 μm.) (*B*) Representative Ca²⁺ responses to light flashes before (green) and during application of 50 μM of the compound indicated below (yellow). (*C*) Compound-induced change in Ca²⁺ baseline (R$_{base}$) measured in $n = 23$ cones in slices obtained from three animals (23/3) for CN02 (CN03, 18/3; CN04, 15/2; CN05, 11/2). Wash shown in gray. (*D* and *E*) Compound-induced changes in area under the curve, with negative values indicating larger response size (*D*), and peak height, with negative values indicating higher peaks (*E*; arbitrary units, a.u.). Statistical comparisons: *C–E*, not-treated WT vs. treated WT using Wilcoxon matched pairs, signed rank test. ΔR, amplitude; GCL, ganglion cell layer; INL, inner nuclear layer containing interneurons; IS, inner segments containing organelles of photoreceptors; ONL, outer nuclear layer containing rod and cone photoreceptor nuclei; OPL, outer plexiform layer; OS, outer segments of photoreceptor cells. n.s., $P > 0.05$; *$P \leq 0.05$, ***$P \leq 0.001$.

Ten cyclic nucleotides were generated and denominated CN01–CN10. Previous work (20–22) had established the R$_4$ oxo-substituted compound CN01 as a PKG and CNGC activator. The phosphorothioates CN02–CN10 were suggested to inhibit PKG. Compounds CN02, CN08, and CN09 were predicted to activate, and the remaining compounds to inhibit, CNGC. The absolute and relative lipophilicity was measured, and the compounds were grouped according to their structural motifs (PET and C-8) (20–22) and their predicted inhibitory patterns (Table 1) and then forwarded to testing in rod photoreceptor-like cell cultures as a prescreen for biological activity (Fig. 1*B*).

Screening of cGMP Analogs in Cell and Tissue Models for RD in Vitro.
Primary rod photoreceptor-like cell cultures were derived from mice carrying the *rd1* mutation in *Pde6b* (16). Here, cells expressing rhodopsin (i.e., rod photoreceptors) undergo spontaneous cell death, with a peak of cell demise at day in vitro

(DIV) 11. Rhodopsin-expressing cells have functional CNGC (16, 25), display increased intracellular cGMP levels compared with WT cells, and express all three PKG isoforms (PKG1α, 1β, and 2; Fig. S1). We used these *rd1* cell cultures as a rapid in vitro compound screening system by exposing them to different cGMP analogs and evaluating their effect on cell death at DIV11 using ethidium homodimer staining (Fig. 2*A* and Fig. S2*A*). For comparison, we tested CN01, the oxo-form of CN02 and activator of PKG and CNGC, which had no effect on cell death. In contrast, the *R*$_P$-configurated sulfur forms (i.e., PKG inhibitors) CN02–CN07 showed significant protective effects at a concentration of 50 μM. At the same time CN08 and CN09 did not protect *rd1* cells, while CN10 was toxic at 50 μM (Fig. 2*B*). Dose–response curves were obtained for CN02–CN07 and were used to calculate the corresponding EC$_{50}$ values (Fig. 2 *C–E*). Remarkably, compounds CN05 and CN07 maintained their protective effects on *rd1* cells down to the pico- and even femtomolar range.

Compounds with significant protective activity on photoreceptor-like cells were validated in organotypic retinal explants. This system permits analysis of direct drug effects on photoreceptor viability while preserving their cytological context, under defined, serum-free conditions (7, 26). We used explants derived from *rd1* mice (Fig. 2*F*), which show prominent rod degeneration at postnatal (P) day 11. The effects of CN02–CN07 on photoreceptor cell death were assessed at P11 using the TUNEL assay. The analysis gave the following rank order of protection: CN04 > CN03 > CN02 > CN05, with CN06 and CN07 having no discernible effect (Fig. 2*G*). The combined information from the cell and tissue levels left us with CN02–CN05 displaying significant photoreceptor neuroprotection.

CN02–CN05 were then tested with respect to inhibition of CNGCs and Ca^{2+} influx in cone photoreceptors. To this end, we used acute, freshly prepared retinal slices from WT animals expressing the TN-XL Ca^{2+} biosensor exclusively in cones (27), monitored by a two-photon Ca^{2+}-imaging approach (28) (Fig. 3*A*). Here, CN02, CN04, and CN05 significantly increased cone Ca^{2+} levels, suggesting CNGC activation. In contrast, CN03 moderately but significantly reduced cone Ca^{2+} levels, likely making it a weak inhibitor of CNGC (Fig. 3 *B* and *C*). Light-induced cone Ca^{2+} responses, as assessed by area under the curve and peak amplitudes, were increased by CN02, decreased by CN03, and remained essentially unchanged by CN04 and CN05 (Fig. 3 *D* and *E*). Overall, these results imply that CN02 and CN03 kept the cone phototransduction cascade and light-induced cone responses largely intact. We later confirmed this interpretation by cone-specific electroretinography (ERG) measurements (discussed below). Because long-term elevation of photoreceptor Ca^{2+} levels is thought to be deleterious (29–31), we selected CN03 as the compound for further investigations.

CN03 Engages PKG and CNGC. To investigate how CN03 exerted its positive effect on photoreceptor survival we analyzed molecular processes downstream of PKG and CNGC activation in *rd1* photoreceptor-like cells (16). PKG phosphorylates target proteins, among them vasodilator-stimulated phosphoprotein (VASP)

at the serine 239 residue (32). Increased phosphorylation at serine 239 was observed specifically in rhodopsin-expressing cells and cells undergoing cell death (Fig. S2 *A* and *B*). Ca^{2+}-activated calpain-type proteases and the nuclear translocation of the calpain substrate and cell death effector AIF are important components of *rd1* degeneration, likely downstream of CNGC activation (16, 33). In cells exposed to CN03 we found reduced serine 239 phosphorylation of VASP together with reduced Ca^{2+} levels (Fig. 4 *A* and *B*), suggesting PKG and CNGC inhibition. We confirmed that CN03 targeted PKG and not PKA by showing that VASP phosphorylation at serine 157, a PKA phosphorylation site, was not affected by the treatment (Fig. S2*C*). CN03 also decreased calpain activation (Fig. 4*C*) and nuclear localization of AIF (Fig. 4*D*). We neither observed signs of toxicity for CN03 at 50 µM on retinal explant cultures derived from WT animals (Fig. 4 *E* and *F*) nor on WT-derived photoreceptor-like cells at concentrations up to 500 µM (Fig. S3 *A* and *B*). *rd1* explant cultures in vitro (Fig. S3*C*) and subsequent in vivo studies in *rd10* animals (Fig. S3*D*) suggested 50 µM CN03 as a suitable treatment dose.

CN03 Protects Photoreceptors Carrying Different Gene Mutations. To assess the protective capacities of CN03 in forms of RD caused by different mutations in the same gene or in a different gene we extended our in vitro testing to retinal explant cultures derived from *rd10* and *rd2* mice. This is important, because the *rd1* mutation in the *Pde6b* gene causes primary rod cell death already during retinal development, with over 50% reduction of the photoreceptor layer until P14 and an almost complete loss of rods by P18 (8, 34). In contrast, the *rd10* mouse harbors a different *Pde6b* mutation, causing slower rod degeneration compared with *rd1*, with around 15% of the photoreceptor layer remaining at P30 (35). The *rd2* (*rds*) mouse carries a mutation in the *Prph2* gene, leading to absence of rod and cone outer segments, with strongly reduced retinal function, but a relatively slow loss of both rods and cones. Around 35% of the *rd2* photoreceptor layer is lost until P60 (36).
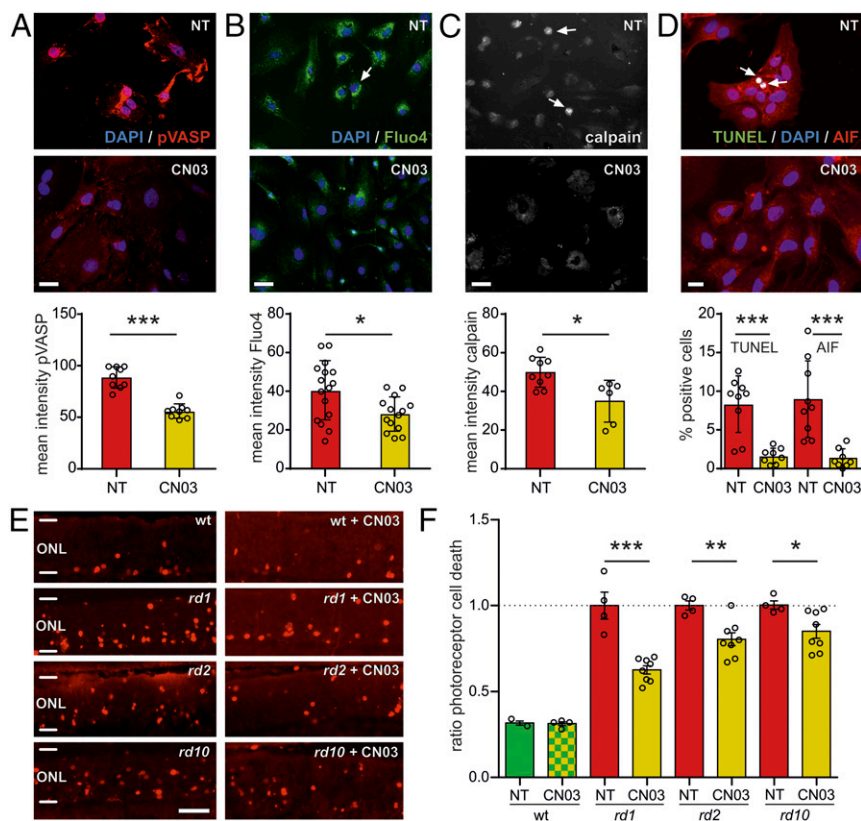
Fig. 4. CN03 acts on PKG and CNGC and reduces photoreceptor death in three different in vitro RD models. (*A*–*D*) Photoreceptor-like cell cultures derived from *rd1* mice (NT, red bars) and effects of 50 µM CN03 (yellow bars) on degeneration markers (*n* = 9–15 cell cultures obtained from three to five independent preparations). (*A*) CN03 reduced the phosphorylation at serine 239 of the PKG-target VASP (pVASP, red). (*B*) Fluo-4, AM Ca^{2+} imaging (green, arrow indicates a cell with high Ca^{2+}) indicated reduction in intracellular Ca^{2+}. (*C*) Calpain protease activity assay brightly labeled condensed dying cells (arrows). Mean calpain labeling intensity was reduced after CN03 treatment. (*D*) AIF (red) translocation from mitochondria to nuclei (blue) and cell death, as assessed by the TUNEL assay (green), was restrained by CN03 treatment (triple-stained nuclei shown in white; see arrows). (*E*) CN03 (50 µM) had no adverse effects in P11 organotypic explants derived from WT (top row). In P11 *rd1*, P19 *rd2*, and P18 *rd10* explants CN03 reduced the number of dying cells in the ONL. (*F*) Quantification of the data from *E*; ratio (treated/NT) of TUNEL-labeled cells (NT WT, *n* = 2 separate retinal explant cultures; CN03 WT, 4; each NT mutant, 4; each CN03 treated mutant, 8; *rd1* data from Fig. 2*G* shown for comparison). Error bars in *A*–*D* and *F*: SEM. Statistical comparisons: Student's *t* test (unpaired, two-tailed). NT, not treated. (Scale bars: *A*–*C*, 50 µm; *D*, 20 µm; *E*, 50 µm.) *$P \leq 0.05$, **$P \leq 0.01$, ***$P \leq 0.001$.
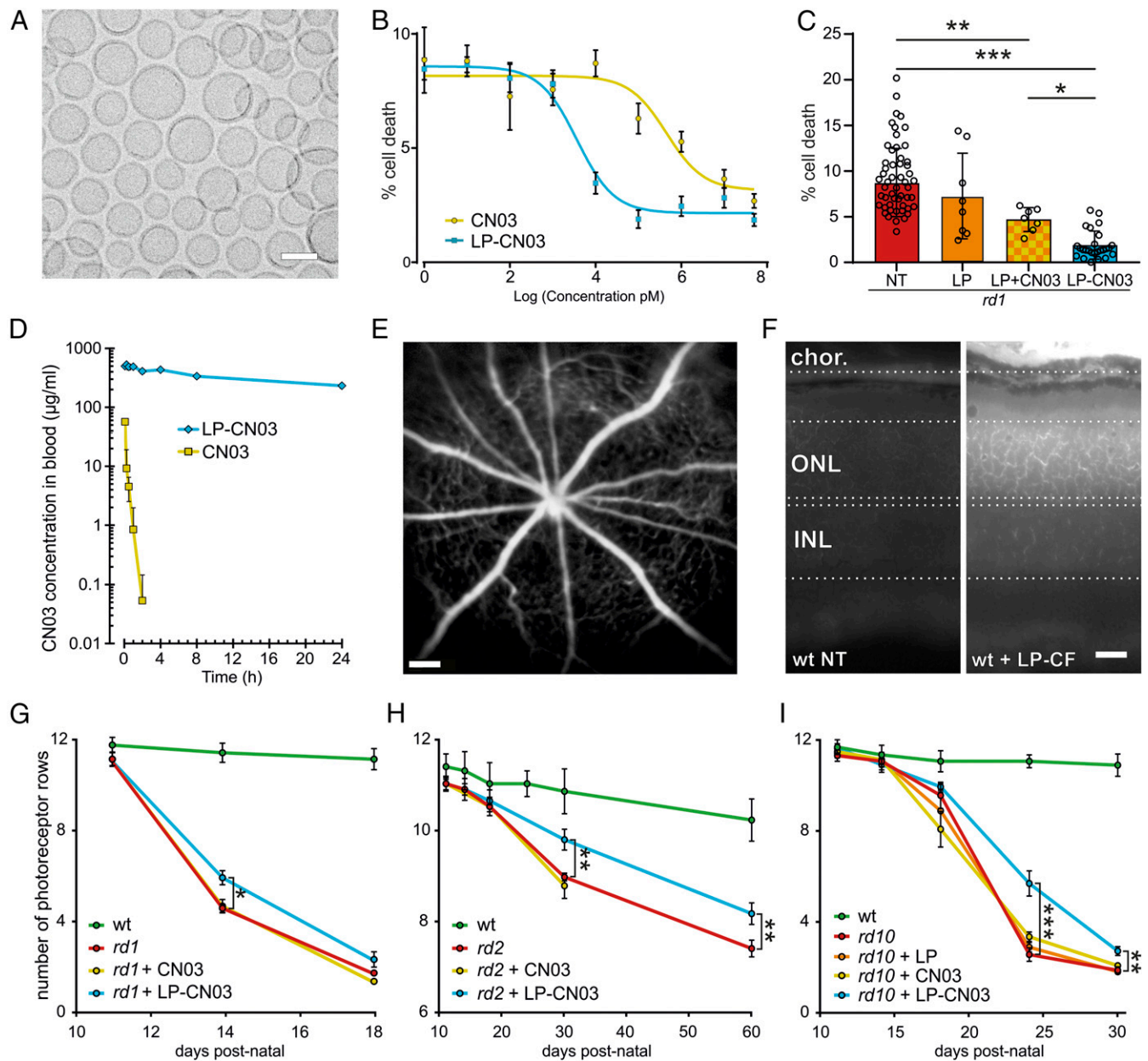
Fig. 5. CN03 liposomal formulation improves neuroprotective efficacy. (*A*) Electron microscopy of GSH-PEG liposomes loaded with CN03 showing a vesicle size of ∼100 nm. (*B*) Neuroprotective effects of CN03 (yellow; EC$_{50}$ = 400 ± 5 nM) and LP-CN03 (blue; EC$_{50}$ = 3.5 ± 1 nM) in *rd1* mutant photoreceptor-like cell cultures (*n* = 9 cell cultures from three independent preparations per concentration/treatment). (*C*) Cell death in NT *rd1* photoreceptor-like cells (red bar), empty liposome treatment (LP, orange), coadministration of LP with free CN03 (LP+CN03, 1 μM; yellow/orange checkered), and LP-CN03 (1 μM). *n* = 8–62 different cell cultures from two to three independent preparations. (*D*) PK study in adult rats comparing in vivo half-life of free CN03 (10 min; yellow) vs. LP-CN03 (24 h; blue). *n* = 6 rats per group. (*E*) In vivo imaging using SLO. P10 WT mice were injected i.p. with carboxyfluorescein-loaded liposomes (LP-CF) and analyzed at P14. Fluorescent label was present mostly in retinal vasculature. (*F*) Cross-sections of P14 retinae from such LP-CF–treated animals displayed fluorescent labeling of choroidal blood vessels (chor.) but also of photoreceptors in ONL. (*G–I*) Three different in vivo RD mouse models were treated with CN03 (yellow), LP only (orange), or LP-CN03 (blue), beginning at the onset of degeneration (P10, *rd1*; P14, *rd2* and *rd10*; cf. Table S2). Photoreceptor survival was assessed on ex vivo retinal tissue sections by counting photoreceptor rows in ONL. WT (green) shown for comparison. *n* = 4–8 animals (one eye per animal) per time point and genotype. (*G*) Progression of photoreceptor degeneration in *rd1* animals (red) compared with *rd1* animals treated with free CN03 (yellow) and LP-CN03 (blue). (*H*) Progression of degeneration in NT vs. LP-CN03–treated *rd2* mice. (*I*) Progression of degeneration in NT (red) or LP-treated (orange) or CN03-treated (yellow) vs. LP-CN03 treated (blue) *rd10* animals. Note different *y* axis scales in *G–I* to account for different degeneration kinetics. Error bars: SEM. Statistical comparisons: *C*, one-way ANOVA and Newman–Keuls multiple comparison test; *G–I*, Student's *t* test (unpaired, two-tailed). INL, inner nuclear layer; NT, not treated. (Scale bars: *A*, 100 nm; *E*, 200 μm; *F*, 25 μm.) *$P \leq 0.05$, **$P \leq 0.01$, ***$P \leq 0.001$.

We found that CN03 protected photoreceptors in both *rd2* and *rd10* retinal explants in vitro (Fig. 4 *E* and *F*), thus generalizing our *rd1* findings. Since rods outnumber cones 97:3 in the mouse retina (37), the protection observed in all three mutants is expected to relate mainly to a preservation of rods.

Liposomal Formulation Facilitates Compound Delivery Across the BRB. A major challenge for in vivo drug delivery to the retina is the BRB (18, 38). To facilitate retinal drug delivery, we chose glutathione-targeted PEGylated (GSH-PEG) liposomes, which had previously been shown to be a safe delivery system that
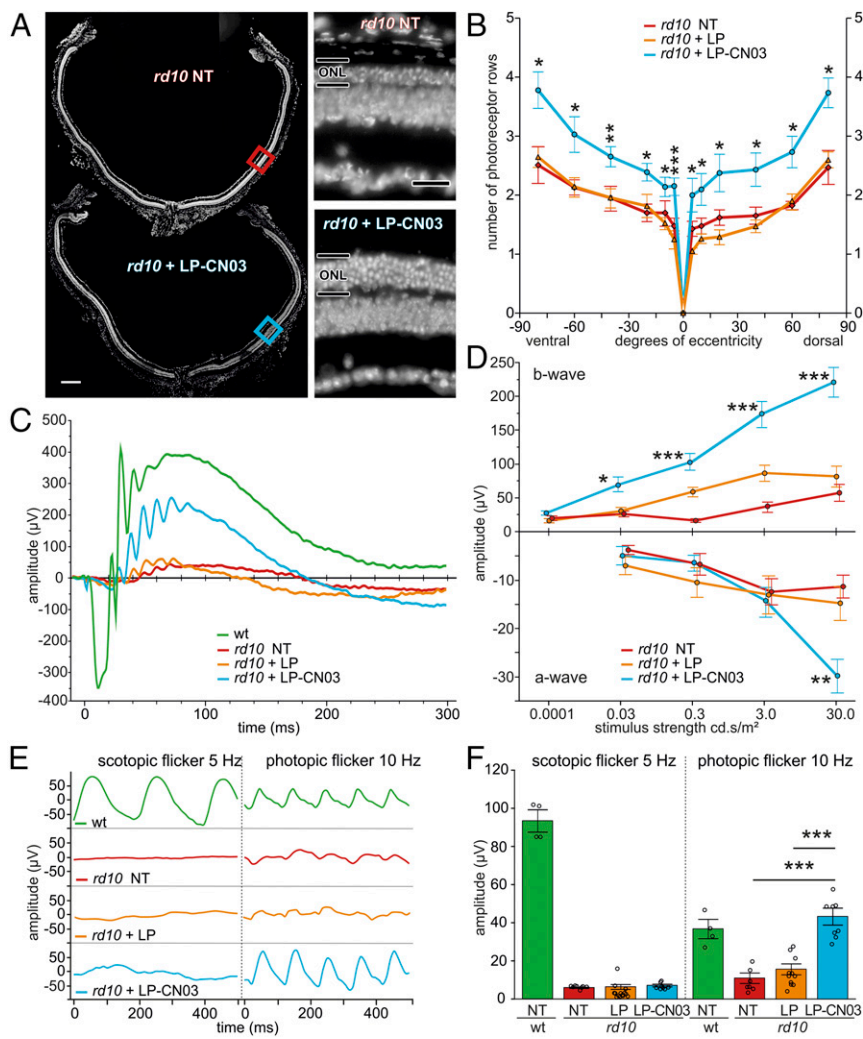
Fig. 6. LP-CN03 partly preserves *rd10* retinal morphology and cone photoreceptor function at P30. (*A*) P30 sagittal retinal cross-sections from NT *rd10* (red) and LP-CN03–treated (blue) *rd10* animals, with insets showing higher magnification. (*B*) Quantification of photoreceptor rows (P30) along the dorsal–ventral axis, from center (optic nerve = 0°) to periphery (90°). Colors as in *A*; empty liposome condition (LP) shown in orange. (*C*) Representative ERG responses (30.0 cd·s/m^2, dark-adapted) in *rd10* animals; NT (red), LP-treated (orange), and LP-CN03–treated (blue). Congenic, age-matched WT traces (green) shown for comparison. (*D*) Summary plots for a- and b-wave maximum amplitudes over different light stimulus intensities. (*E*) Rod and cone flicker ERG responses elicited by either 5-Hz scotopic flicker (0.000122 cd·s/m^2) or 10-Hz photopic flicker (30 cd·s/m^2). (*F*) Comparison of Fourier-transformed scotopic- and photopic-flicker ERGs. Error bars: SEM. WT: $n = 4$ animals; *rd10*: $n = 8–12$ per condition (one eye per animal). Statistical comparisons: *B*, Student's *t* test (unpaired, two-tailed) comparing LP-CN03 vs. LP treatment; *D* and *F*, one-way ANOVA with Tukey's honestly significant difference post hoc test; NT, not treated. (Scale bars: *A*, 200 μm; *A, Inset*, 50 μm.) *$P ≤ 0.05$, **$P ≤ 0.01$, ***$P ≤ 0.001$.

favors the transport of cargo across the blood–brain barrier after systemic administration (19, 39). We refer to GSH-PEG liposome-encapsulated CN03 as LP-CN03 (Fig. 5*A*). The protective capacity of this nanosized compound formulation was initially tested in *rd1* photoreceptor-like cell cultures in vitro, where LP-CN03 (EC$_{50}$ = 3.5 ± 1 nM) was around 100-fold more effective than free CN03 (EC$_{50}$ = 400 ± 5 nM) in reducing *rd1* cell death (Fig. 5*B*). This remarkable increase in efficacy was likely due to CN03's being encapsulated into GSH-PEG liposomes, because empty liposomes alone had no consistent effect, and free CN03 mixed with empty liposomes was significantly less effective than LP-CN03 (Fig. 5*C*).

Next, we compared the in vivo bioavailability of CN03 in free form and liposomal formulation after i.v. injection in WT rats, an established standard for pharmacokinetic (PK) studies. The half-life of the free CN03 compound in the blood stream was only about 10 min, presumably because of a rapid excretion of cyclic nucleotides via the renal system (40, 41). Encapsulation of CN03 in liposomes (LP-CN03) prolonged in vivo half-life in the blood stream to more than 24 h (Fig. 5*D*).

The efficacy of GSH-PEG liposomes for in vivo delivery to the neuroretina was assessed by i.p. administration of liposomes loaded with carboxyfluorescein, followed by in vivo imaging with scanning laser ophthalmoscopy (SLO). Four days after a single i.p. injection, fluorescence was still clearly detectable in the retina (Fig. 5*E*). In retinal cross-sections carboxyfluorescein strongly labeled choroidal blood vessels, and the retina, especially the outer nuclear layer (ONL), confirming successful delivery of liposomal

contents to the photoreceptors (Fig. 5*F*). We routinely monitored LP-CN03–treated mice and rats in vivo and postmortem (*Materials and Methods*) but could not find any macroscopic evidence for toxic effects. Likewise, postnatal weight gains during a 2-mo-long LP-CN03 administration were normal in both mice and rats (Fig. S3 *E* and *F*).

Systemic Delivery of LP-CN03 Protects Photoreceptors in Three Murine RD Models in Vivo. To evaluate in vivo protective effects we administered the LP-CN03 systemically via i.p. injections starting at the respective onset of degeneration in each model and counted the number of photoreceptor rows on ex vivo retinal sections (Fig. 5 *G–I* and Fig. S3 *G–I*). In *rd1* mice, systemic administration of free CN03 (starting at P10, once per day) had no effect on photoreceptor survival at P14, whereas treatment with LP-CN03 significantly increased photoreceptor numbers (Fig. 5*G* and Fig. S3*G*). Also, in the more slowly degenerating *rd2* and *rd10* models treatment with LP-CN03 (starting at P14, once per day in *rd10* and every second day in *rd2*) resulted in a significant increase in the number of surviving photoreceptor rows, compared with untreated mutant, free CN03, or LP only (Fig. 5 *H* and *I* and Fig. S3 *H* and *I*). LP-CN03 preserved *rd2* retina structurally and functionally at P30 and P60 (Fig. S4). In relative terms, the protection observed was more striking in *rd10* animals, which motivated us to evaluate this model in more detail. We analyzed sagittal sections of P30 *rd10* retina (Fig. 6*A*) to survey the number of surviving photoreceptor rows as a function of eccentricity (i.e., distance from the optic nerve).

Table 2. Results of one-way ANOVA analysis conducted for each ERG stimulus condition

ERG amplitude	WT			rd10 NT			rd10 + LP			rd10 + LP-CN03			df	F	P
	n	Mean, μV	SD, μV	n	Mean, μV	SD, μV	n	Mean, μV	SD, μV	n	Mean, μV	SD, μV			
Scotopic single flash 0.0001															
b-wave				8	19.85	12.54	7	16.15	11.36	8	27.45	12.96	(2, 22)	1.65	ns
Scotopic single flash 0.03															
a-wave				8	−3.74	3.38	6	−7.00	4.97	8	−4.93	7.60	(2, 21)	0.57	ns
b-wave				8	26.07	15.84	7	29.96	20.41	8	69.94	43.92	(2, 22)	5.23	0.0149*
Scotopic single flash 0.3															
a-wave				8	−6.71	8.33	5	−11.44	7.44	8	−6.48	6.09	(2, 20)	0.83	ns
b-wave				8	16.40	6.57	7	58.48	22.04	8	103.18	48.18	(2, 22)	15.48	<0.0001***
Scotopic single flash 3.0															
a-wave				7	−12.39	7.73	7	−15.77	14.38	8	−14.58	12.47	(2, 21)	0.16	ns
b-wave				8	36.09	22.94	7	86.26	36.73	8	173.09	71.07	(2, 22)	16.27	<0.0001***
Scotopic single flash 30															
a-wave				8	−11.31	7.71	5	−14.82	10.16	8	−29.85	14.08	(2, 20)	6.10	0.0095**
b-wave				8	57.36	38.05	7	81.35	55.78	8	220.80	83.16	(2, 22)	15.94	<0.0001***
Photopic single flash 3.0															
a-wave				7	−2.54	3.96	6	−6.39	7.91	8	−5.16	5.27	(2, 20)	0.77	ns
b-wave				7	26.38	10.32	7	38.34	20.45	8	81.67	29.12	(2, 21)	13.46	0.0002***
Scotopic 5-Hz flicker	4	93.37	11.73	8	6.02	0.94	14	6.45	4.75	8	7.20	2.00	(3, 30)	359.87	<0.0001***
Photopic 10-Hz flicker	4	36.82	10.14	7	11.01	7.28	11	15.68	9.48	8	43.33	12.59	(3, 29)	18.33	<0.0001***

Comparison of LP-CN03 effects on ERG amplitudes at P30 in WT and rd10 mice, not treated (NT), treated with empty liposome (LP), or LP-CN03, respectively. ns: $P > 0.05$, *$P \leq 0.05$, **$P \leq 0.01$, ***$P \leq 0.001$.

Throughout the sagittal axis of LP-CN03–treated *rd10* mice photoreceptor survival was increased by at least 50%, compared with animals that were treated with LP alone (Fig. 6*B*). Loss of photoreceptors in untreated and LP-treated *rd10* mice was similar.

We then evaluated the effect of LP-CN03 on *rd10* retinal function in vivo using ERG. At P30, standard ERG responses to single-flashes (30.0 cd·s/m^2), recorded in dark-adapted WT mice, measured from −350 μV (a-wave; primary photoreceptor response) to +400 μV (b-wave; secondary inner retinal activity, mainly bipolar cells). ERG responses of untreated *rd10* animals of the same age were much smaller, measuring from ∼−10 μV to ∼+50 μV (Fig. 6*C*). Treatment with LP alone had no detectable effect on *rd10* ERG responses. In contrast, LP-CN03 strongly and significantly increased both a-wave (−30 μV, for the highest light level) and b-wave responses (+250 μV) in *rd10* animals. The clearly discernible a-wave in *rd10* treated animals confirmed that CN03 did not impede cone phototransduction. Across different light intensities, b-wave amplitudes were four- to fivefold larger in LP-CN03–treated *rd10* animals (Fig. 6*D* and Tables 2 and 3).

A comparison between our data and previously reported ERG recordings from Rho$^{−/−}$ mice (42), in which only cones are functional, suggests that cone function was almost completely preserved in treated *rd10* mice. To investigate this further, we recorded scotopic (rod-driven) and photopic (cone-driven) flicker ERGs. As expected for animals with dysfunctional rods (due to *Pde6b* mutation), scotopic flicker responses in *rd10*— whether treated or not—were completely abolished (Fig. 6*E*). Strikingly, photopic flicker responses in LP-CN03 *rd10* treated animals appeared even larger than in WT (Fig. 6 *E* and *F* and Table 3). A likely explanation is that with nonfunctional *rd10* rods the cone-driven OFF-bipolar cell channel lacks inhibitory input from the rod pathway, resulting in a higher net cone response to flicker (42). Taken together, our ERG results support evidence that LP-CN03 treatment preserved *rd10* cone function through inhibition of rod cell death.

Discussion

Here, we provide proof of principle that cGMP analogs can counteract photoreceptor degeneration in vivo when delivered across the BRB to their cellular target. We also demonstrate that the preservation of rods can improve the function of cones, lending support to the hypothesis that "sparing the rods" indeed "saves the cones" (4).

Dysregulation of cGMP has been observed in a variety of diseases, including neurodegeneration (34, 43, 44) and RD, where it seems to be a common disease denominator (11). High levels of cGMP likely cause abnormal PKG and/or CNGC activity (17). PKG appears as an important mediator of cGMP-dependent cell death, and its overactivation is known to cause loss of cellular adhesion and a form of cell death reminiscent of anoikis (45, 46). Our data show that PKG inhibition has strong neuroprotective effects on postmitotic photoreceptors, thus corroborating earlier findings on this theme, for instance where reduced PKG activity increased the neuronal tolerance to stress (47). Follow-up studies may shed further light on how PKG inhibition affects downstream processes and how these may promote photoreceptor survival.

With respect to the CNGC, high cGMP levels causing a dangerous inflow of Ca^{2+} have long since been proposed as a key event in photoreceptor degeneration (29). While recent data indicate that the Ca^{2+} dynamics rather than the absolute intracellular Ca^{2+} concentrations may be more relevant for the degeneration of cones in mice (48), there is a general consensus that excessive Ca^{2+} influx over prolonged periods of time (i.e., in a chronic disease) is detrimental (15, 49). An interesting point for future studies would be to see if cGMP analogs can selectively inhibit any of the rod or cone CNGC subunits.

The fact that cGMP analogs can be tailored to limit the activity of PKG and/or CNGC makes this class of compounds very promising for a targeted therapy of RD. Indeed, we found that CN03 inhibited both PKG and CNGC, probably explaining why this compound performed so well in our test systems. In contrast, and against prior expectations (22), CN04 and CN05 behaved as CNGC activators, suggesting that their large R$_3$ substituents overruled the CNGC inhibitory effect of the R$_1$ + R$_2$ PET substitution. This may also explain the lack of protection by the dimers CN09 and CN10 with their large-molecular-size R$_3$ substituent, linking the two cGMPS moieties.

Another aspect of our study is the administration route of drugs to the retina. In current clinical practice most drugs targeting retinal cells are locally injected into the vitreous body,

Table 3. Post hoc analysis using Tukey's honestly significant difference test on all possible pairwise contrasts for each stimulus condition

ERG amplitude	Pair		Least significant mean difference			
			Mean, µV	SD, µV	CI, µV	P
Scotopic single flash 0.03						
b-wave	rd10 + LP-CN03	rd10 NT	43.87	14.90	[6.18, 81.56]	0.0209*
	rd10 + LP-CN03	rd10 + LP	39.98	15.42	[0.96, 78.99]	0.0440*
	rd10 + LP	rd10 NT	3.89	15.42	[−35.12, 42.91]	ns
Scotopic single flash 0.3						
b-wave	rd10 + LP-CN03	rd10 NT	86.78	15.60	[47.32, 126.24]	<0.0001***
	rd10 + LP-CN03	rd10 + LP	44.70	16.15	[3.86, 85.55]	0.0305*
	rd10 + LP	rd10 NT	42.07	16.15	[1.23, 82.92]	0.0428*
Scotopic single flash 3.0						
b-wave	rd10 + LP-CN03	rd10 NT	137.00	24.27	[75.59, 198.41]	<0.0001***
	rd10 + LP-CN03	rd10 + LP	86.83	25.13	[23.26, 150.39]	0.0067**
	rd10 + LP	rd10 NT	50.17	25.13	[−13.39, 113.74]	ns
Scotopic single flash 30						
a-wave	rd10 NT	rd10 + LP-CN03	18.54	5.55	[4.38, 32.70]	0.0097**
	rd10 + LP	rd10 + LP-CN03	15.03	6.33	[−1.11, 31.18]	ns
	rd10 NT	rd10 + LP	3.51	6.33	[−12.64, 19.65]	ns
b-wave	rd10 + LP-CN03	rd10 NT	163.44	31.07	[84.85, 242.04]	0.0001***
	rd10 + LP-CN03	rd10 + LP	139.45	32.16	[58.10, 220.81]	0.0009**
	rd10 + LP	rd10 NT	23.99	32.16	[−57.36, 105.35]	ns
Scotopic 5-Hz flicker	WT	rd10 NT	87.35	3.04	[79.08, 95.62]	<0.0001***
	WT	rd10 + LP	86.92	2.82	[79.27, 94.58]	<0.0001***
	WT	rd10 + LP-CN03	86.17	3.04	[77.91, 94.44]	<0.0001***
	rd10 + LP-CN03	rd10 NT	1.18	2.48	[−5.57, 7.93]	ns
	rd10 + LP-CN03	rd10 + LP	0.75	2.20	[−5.24, 6.73]	ns
	rd10 + LP	rd10 NT	0.43	2.20	[−5.55, 6.41]	ns
Photopic 10-Hz flicker	rd10 + LP-CN03	rd10 NT	32.32	5.21	[18.03, 46.61]	<0.0001***
	rd10 + LP-CN03	rd10 + LP	27.65	4.68	[14.82, 40.49]	<0.0001***
	WT	rd10 NT	25.81	6.31	[8.50, 43.12]	0.0020**
	WT	rd10 + LP	21.15	5.88	[5.02, 37.27]	0.0068**
	rd10 + LP-CN03	WT	6.51	6.16	[−10.40, 23.42]	ns
	rd10 + LP	rd10 NT	4.67	4.87	[−8.69, 18.02]	ns

ns: P > 0.05, *P ≤ 0.05, **P ≤ 0.01, ***P ≤ 0.001; LP, empty liposome; NT, not treated.

where they need to cross the BRB to exert their effects (50). Repeated intraocular injections carry a cumulative risk for serious adverse effects, most notably endophthalmitis (51). Systemic administration can be considered less risky for the eye as well as more patient-friendly. Nevertheless, to avoid any hazards associated with systemic exposure, local application of CN03 to the eye is also a viable option. Besides the delivery as liposomal formulation it may be possible to combine CN03 with alternative drug delivery systems, such as poly(lactic-*co*-glycolic acid) for intraocular slow release (52) or cyclodextrins for topical delivery (53). Furthermore, the marked prolongation of its in vivo half-life with liposomal encapsulation, and the lack of therapeutic effect without, are in line with previous observations (19, 39) and our findings thus stress the importance of efficient drug delivery for the treatment of retinal diseases. Whether the efficacy of the liposomal formulation stems predominantly from the extension of in vivo half-life or from the improved BRB permeability needs to be addressed in future studies that may use, for instance, in vivo steady-state i.v. dosing. We also propose that our pharmacological treatment may be combined with recently developed gene therapy approaches (54, 55) both to enhance prosurvival treatment effects and to extend the treatment window of opportunity for gene therapy.

In summary, we suggest cGMP signaling as a common target for the treatment of genetically and phenotypically divergent types of RD. Testing in other animal models, such as *Pde6a* mutants (8), could further extend the spectrum of RD genes that may be treatable with inhibitory cGMP analogs. We have pro-

duced structures with unique and target-specific properties and can now promote cyclic nucleotide analogs as a class of pharmacologically active compounds for the treatment of RD. The value of this concept for clinical translation is supported by an orphan drug designation for CN03, awarded by the European Medicines Agency (EU/3/15/1462). Moreover, we have adapted a nanoscale liposomal drug delivery vehicle to innovatively and efficiently target the retinal photoreceptors in vivo. Indeed, we demonstrate that drug delivery is a key factor for achieving in vivo therapeutic success. Our approach preserves retinal function in relevant animal models, highlighting its therapeutic potential for genetically diverse and currently untreatable blinding diseases.

Materials and Methods

For details on the chemical synthesis of cGMP analogs, determination of their lipophilicity, and liposomal encapsulation please refer to *SI Materials and Methods*. The general work flow for the in vitro and in vivo testing of cGMP analogs is given in Fig. 1*B*. Further details on animals, in vitro cell and retinal explant cultures, Ca^{2+} imaging, in vivo PKs, in vivo imaging and function testing, as well as on statistical analysis are given in *SI Materials and Methods*.

Animals for preparation of primary retinal cell cultures were kept at Centro Servizi Stabulario Interdipartimentale of the University of Modena and Reggio Emilia. The protocol was approved by the Ethical Committee of the University of Modena and Reggio Emilia (protocol no. 106 22/11/2012) and by the Italian Ministero della Salute (346/2015-PR). Animals for in vitro retinal explant studies were kept at the animal facilities of the Biomedical Centre, Lund University. All procedures were evaluated by the local animal care and ethics committees and performed in accordance with permits M172-12, M191-14, and M92-15. Efforts were made to keep the number of

animals used and their suffering to a minimum. Animals for in vivo studies were kept in the Tübingen Institute for Ophthalmic Research animal housing facility. All in vivo procedures were performed in accordance with the local ethics committee at Tübingen University (§4 registrations from 29 to 04-10; 30-06-10; 11-03-11; animal permit AK5/12) and the Association for Research in Vision and Ophthalmology statement for the use of animals in ophthalmic and visual research.

1. Berger W, Kloeckener-Gruissem B, Neidhardt J (2010) The molecular basis of human retinal and vitreoretinal diseases. *Prog Retin Eye Res* 29:335–375.
2. Sahel JA, Marazova K, Audo I (2014) Clinical characteristics and current therapies for inherited retinal degenerations. *Cold Spring Harb Perspect Med* 5:a017111.
3. Kennan A, Aherne A, Humphries P (2005) Light in retinitis pigmentosa. *Trends Genet* 21:103–110.
4. Curcio CA, Owsley C, Jackson GR (2000) Spare the rods, save the cones in aging and age-related maculopathy. *Invest Ophthalmol Vis Sci* 41:2015–2018.
5. Lucas KA, et al. (2000) Guanylyl cyclases and signaling by cyclic GMP. *Pharmacol Rev* 52:375–414.
6. Farber DB, Lolley RN (1974) Cyclic guanosine monophosphate: Elevation in degenerating photoreceptor cells of the C3H mouse retina. *Science* 186:449–451.
7. Paquet-Durand F, Hauck SM, van Veen T, Ueffing M, Ekström P (2009) PKG activity causes photoreceptor cell death in two retinitis pigmentosa models. *J Neurochem* 108:796–810.
8. Sanyal S, Bal AK (1973) Comparative light and electron microscopic study of retinal histogenesis in normal and rd mutant mice. *Z Anat Entwicklungsgesch* 142:219–238.
9. Sakamoto K, McCluskey M, Wensel TG, Naggert JK, Nishina PM (2009) New mouse models for recessive retinitis pigmentosa caused by mutations in the Pde6a gene. *Hum Mol Genet* 18:178–192.
10. Xu J, et al. (2013) cGMP accumulation causes photoreceptor degeneration in CNG channel deficiency: Evidence of cGMP cytotoxicity independently of enhanced CNG channel function. *J Neurosci* 33:14439–14948.
11. Arango-Gonzalez B, et al. (2014) Identification of a common non-apoptotic cell death mechanism in hereditary retinal degeneration. *PLoS One* 9:e112142.
12. Ramamurthy V, Niemi GA, Reh TA, Hurley JB (2004) Leber congenital amaurosis linked to AIPL1: A mouse model reveals destabilization of cGMP phosphodiesterase. *Proc Natl Acad Sci USA* 101:13897–13902.
13. Iribarne M, Masai I (2017) Neurotoxicity of cGMP in the vertebrate retina: From the initial research on rd mutant mice to zebrafish genetic approaches. *J Neurogenet* 31:88–101.
14. Paquet-Durand F, et al. (2011) A key role for cyclic nucleotide gated (CNG) channels in cGMP-related retinitis pigmentosa. *Hum Mol Genet* 20:941–947.
15. Orrenius S, Zhivotovsky B, Nicotera P (2003) Regulation of cell death: The calcium-apoptosis link. *Nat Rev Mol Cell Biol* 4:552–565.
16. Sanges D, Comitato A, Tammaro R, Marigo V (2006) Apoptosis in retinal degeneration involves cross-talk between apoptosis-inducing factor (AIF) and caspase-12 and is blocked by calpain inhibitors. *Proc Natl Acad Sci USA* 103:17366–17371.
17. Wang T, Tsang SH, Chen J (2017) Two pathways of rod photoreceptor cell death induced by elevated cGMP. *Hum Mol Genet* 26:2299–2306.
18. Campbell M, et al. (2011) Systemic low-molecular weight drug delivery to pre-selected neuronal regions. *EMBO Mol Med* 3:235–245.
19. Rip J, et al. (2014) Glutathione PEGylated liposomes: Pharmacokinetics and delivery of cargo across the blood-brain barrier in rats. *J Drug Target* 22:460–467.
20. Butt E, Eigenthaler M, Genieser HG (1994) (Rp)-8-pCPT-cGMPS, a novel cGMP-dependent protein kinase inhibitor. *Eur J Pharmacol* 269:265–268.
21. Butt E, Pöhler D, Genieser HG, Huggins JP, Bucher B (1995) Inhibition of cyclic GMP-dependent protein kinase-mediated effects by (Rp)-8-bromo-PET-cyclic GMPS. *Br J Pharmacol* 116:3110–3116.
22. Wei JY, Cohen ED, Yan YY, Genieser HG, Barnstable CJ (1996) Identification of competitive antagonists of the rod photoreceptor cGMP-gated cation channel: Beta-phenyl-1,N2-etheno-substituted cGMP analogues as probes of the cGMP-binding site. *Biochemistry* 35:16815–16823.
23. Kramer RH, Tibbs GR (1996) Antagonists of cyclic nucleotide-gated channels and molecular mapping of their site of action. *J Neurosci* 16:1285–1293.
24. Kramer RH, Karpen JW (1998) Spanning binding sites on allosteric proteins with polymer-linked ligand dimers. *Nature* 395:710–713.
25. Demontis GC, Aruta C, Comitato A, De Marzo A, Marigo V (2012) Functional and molecular characterization of rod-like cells from retinal stem cells derived from the adult ciliary epithelium. *PLoS One* 7:e33338.
26. Caffé AR, et al. (2001) Mouse retina explants after long-term culture in serum free medium. *J Chem Neuroanat* 22:263–273.
27. Wei T, et al. (2012) Light-driven calcium signals in mouse cone photoreceptors. *J Neurosci* 32:6981–6994.
28. Kulkarni M, et al. (2015) Imaging Ca2+ dynamics in cone photoreceptor axon terminals of the mouse retina. *J Vis Exp* e52588.
29. Fox DA, Poblenz AT, He L (1999) Calcium overload triggers rod photoreceptor apoptotic cell death in chemical-induced and inherited retinal degenerations. *Ann N Y Acad Sci* 893:282–285.
30. Trifunović D, et al. (2012) Neuroprotective strategies for the treatment of inherited photoreceptor degeneration. *Curr Mol Med* 12:598–612.
31. Frasson M, et al. (1999) Retinitis pigmentosa: Rod photoreceptor rescue by a calcium-channel blocker in the rd mouse. *Nat Med* 5:1183–1187.
32. Deguchi A, et al. (2002) Vasodilator-stimulated phosphoprotein (VASP) phosphorylation provides a biomarker for the action of exisulind and related agents that activate protein kinase G. *Mol Cancer Ther* 1:803–809.
33. Paquet-Durand F, et al. (2006) Calpain is activated in degenerating photoreceptors in the rd1 mouse. *J Neurochem* 96:802–814.
34. Sahaboglu A, et al. (2013) Retinitis pigmentosa: Rapid neurodegeneration is governed by slow cell death mechanisms. *Cell Death Dis* 4:e488.
35. Gargini C, Terzibasi E, Mazzoni F, Strettoi E (2007) Retinal organization in the retinal degeneration 10 (rd10) mutant mouse: A morphological and ERG study. *J Comp Neurol* 500:222–238.
36. Sanyal S, Jansen HG (1981) Absence of receptor outer segments in the retina of rds mutant mice. *Neurosci Lett* 21:23–26.
37. Jeon CJ, Strettoi E, Masland RH (1998) The major cell populations of the mouse retina. *J Neurosci* 18:8936–8946.
38. Gaillard PJ, Visser CC, Appeldoorn CC, Rip J (2012) Targeted blood-to-brain drug delivery–10 key development criteria. *Curr Pharm Biotechnol* 13:2328–2339.
39. Lindqvist A, Rip J, Gaillard PJ, Björkman S, Hammarlund-Udenaes M (2013) Enhanced brain delivery of the opioid peptide DAMGO in glutathione pegylated liposomes: A microdialysis study. *Mol Pharm* 10:1533–1541.
40. Coulson R, Baraniak J, Stec WJ, Jastorff B (1983) Transport and metabolism of N6- and C8-substituted analogs of adenosine 3',5'-cyclic monophosphate and adenosine 3'5'-cyclic phosphorothioate by the isolated perfused rat kidney. *Life Sci* 32:1489–1498.
41. Propper DJ, et al. (1999) Phase I study of the novel cyclic AMP (cAMP) analogue 8-chloro-cAMP in patients with cancer: Toxicity, hormonal, and immunological effects. *Clin Cancer Res* 5:1682–1689.
42. Tanimoto N, et al. (2015) Electroretinographic assessment of rod- and cone-mediated bipolar cell pathways using flicker stimuli in mice. *Sci Rep* 5:10731.
43. Bollen E, Prickaerts J (2012) Phosphodiesterases in neurodegenerative disorders. *IUBMB Life* 64:965–970.
44. Jaumann M, et al. (2012) cGMP-Prkg1 signaling and Pde5 inhibition shelter cochlear hair cells and hearing function. *Nat Med* 18:252–259.
45. Hou Y, et al. (2006) A role for cyclic-GMP dependent protein kinase in anoikis. *Cell Signal* 18:882–888.
46. Ali M, Rogers LK, Pitari GM (2015) Serine phosphorylation of vasodilator-stimulated phosphoprotein (VASP) regulates colon cancer cell survival and apoptosis. *Life Sci* 123:1–8.
47. Caplan SL, Milton SL, Dawson-Scully K (2013) A cGMP-dependent protein kinase (PKG) controls synaptic transmission tolerance to acute oxidative stress at the Drosophila larval neuromuscular junction. *J Neurophysiol* 109:649–658.
48. Kulkarni M, Trifunović D, Schubert T, Euler T, Paquet-Durand F (2016) Calcium dynamics change in degenerating cone photoreceptors. *Hum Mol Genet* 25:3729–3740.
49. Marambaud P, Dreses-Werringloer U, Vingtdeux V (2009) Calcium signaling in neurodegeneration. *Mol Neurodegener* 4:20.
50. Meyer CH, Krohne TU, Charbel Issa P, Liu Z, Holz FG (2016) Routes for drug delivery to the eye and retina: Intravitreal injections. *Dev Ophthalmol* 55:63–70.
51. Rayess N, et al. (2015) Incidence and clinical features of post-injection endophthalmitis according to diagnosis. *Br J Ophthalmol* 100:1058–1061.
52. Lin H, et al. (2016) Drug delivery nanoparticles: Toxicity comparison in retinal pigment epithelium and retinal vascular endothelial cells. *Semin Ophthalmol* 31:1–9.
53. Loftsson T, Hreinsdóttir D, Stefánsson E (2007) Cyclodextrin microparticles for drug delivery to the posterior segment of the eye: Aqueous dexamethasone eye drops. *J Pharm Pharmacol* 59:629–635.
54. Byrne LC, et al. (2015) Viral-mediated RdCVF and RdCVFL expression protects cone and rod photoreceptors in retinal degeneration. *J Clin Invest* 125:105–116.
55. Xiong W, MacColl Garfinkel AE, Li Y, Benowitz LI, Cepko CL (2015) NRF2 promotes neuronal survival in neurodegeneration and acute nerve damage. *J Clin Invest* 125:1433–1445.